Research article

Efficient removal of bisphenol A from wastewaters: Catalytic wet air oxidation with Pt catalysts supported on Ce and Ce–Ti mixed oxides

Anne Heponiemi[1],*, Said Azalim[2], Tao Hu[1], Tuomas Vielma[3] and Ulla Lassi[1,3]

[1] Research Unit of Sustainable Chemistry, University of Oulu, P.O. Box 4300, FI-90014 Oulu, Finland
[2] Department of Physics, St. John's University, 8000 Utopia Parkway, Queens, NY 11439, USA
[3] Kokkola University Consortium Chydenius, University of Jyväskylä, P.O. Box 567, FI-67701 Kokkola, Finland

* **Correspondence:** Email: anne.heponiemi@oulu.fi; Tel: +358505715560.

Abstract: Catalytic wet air oxidation (CWAO) of an aqueous solution of bisphenol A (BPA) was investigated at 160 °C and 2.0 MPa of air in a batch reactor. Activity of supported platinum catalysts (2.5 wt%), prepared by wet impregnation, was compared with pure cerium and cerium–titanium oxide catalysts. Supported platinum catalysts showed higher activities in the removal of BPA than pure CeO_2, $Ce_{0.8}Ti_{0.2}O_2$ and $Ce_{0.2}Ti_{0.8}O_2$. The oxidation reaction was followed the pseudo-first order rate law and the highest BPA removal, 97% and 95%, was achieved with Pt/CeO_2 and $Pt/Ce_{0.8}Ti_{0.2}O_2$ catalysts respectively. The CWAO of BPA aqueous solution was not a surface area specific reaction but the more important factor affecting the activity of studied catalysts was the amount of chemisorbed oxygen of these samples.

Keywords: CWAO; bisphenol A; platinum; cerium–titanium; XPS

1. Introduction

Bisphenol A (BPA), 2,2-(4,4-dihydroxydiphenyl) propane, is used as an intermediate in the production of polycarbonate and epoxy resins. Final products include adhesives, protective coatings, powder paints, building materials and many other everyday items [1]. BPA is classified as an endocrine disrupting chemical (EDC) which has been reported to affect sexual development and is associated with abnormal feminizing responses in animals and possibly in humans [2–4]. BPA can

enter the environment via manufacturing and processing but also from used plastic materials which have been disposed in landfill [1,5]. Usually the amount of BPA in surface water is rather low and typically the concentration range is from 30 ng L^{-1} to 50 μg L^{-1} [6,7]. Significantly higher BPA concentrations have been observed in ground water situated near landfills. Research performed near a landfill site in Osaka (Japan) showed that a BPA content of 740 μg L^{-1} [8], and 3.6 mg L^{-1} BPA was detected in the analysis of raw landfill leachate taken from West Germany [9]. On the contrary, considerably high BPA concentrations have been found in industrial sewages. In a study on BPA contamination in Canada, the mean concentration of BPA in raw sewage sludge was 37 mg kg^{-1} [10].

According to several studies related to the toxicity of BPA to animals and humans, the need for an effective treatment method for the destruction of BPA in contaminated waters is essential. Conventional biological methods are widely used in the treatment of organic pollutants in wastewater, however, biological methods based on the activated sludge technique require quite long residence time and large-scale treatment plants. In addition, biological methods are not capable to treat phenolic compounds such as BPA from wastewaters [11,12] while the adsorption of BPA onto activated sludge can cause further problems in sludge management [13,14].

Recently, several oxidation techniques such as photocatalysis, ozonation, catalytic wet peroxide oxidation and catalytic wet air oxidation have been used for the degradation of BPA from aqueous solutions [15–18]. One of the most interesting of these techniques, catalytic wet air oxidation (CWAO), is capable of mineralizing organic compounds of wastewater at elevated temperatures (130–200 °C) and pressures (0.5–5.0 MPa) in the presence of a catalyst to intermediates, CO_2 and water [19]. Numerous homogeneous and heterogeneous catalysts have been tested in the CWAO technique. Homogeneous transition metal catalysts such as copper (Ciba-Geigy) and iron (LOPROX) salts are used in commercialized processes by Granit and Bayer respectively [20]. However, the homogeneous process always needs the additional separation step to recycle the catalyst which makes the heterogeneous catalysts using wet air oxidation technique more interesting and cost-efficient. A wide variety of heterogeneous catalysts have been studied in CWAO. Transition metals such as Cu, Ni, Fe, Mn, Co, Ce, Ti, Zr and related mixed oxides have been successfully used in CWAO of several model compounds (e.g., phenol, acetic acid) and also for industrial wastewaters originating, for example, from olive oil and the pulp & paper industry [21–28]. However, leaching of these metal oxides have been detected in oxidized effluents. Noble metals (Pt, Ru, Pd) supported on CeO_2, ZrO_2 and TiO_2 have been found to be the most efficient catalysts in the treatment of organic effluents with CWAO [29]. Especially Ru and Pt supported on Ce–Zr or Ce–Ti mixed oxides have been observed to be more effective than noble metals on pure oxides in the abatement of organic compounds from aqueous solutions [22,30,31].

The novelty of this research is the use of platinum catalysts supported on cerium oxide and cerium–titanium mixed oxides in the catalytic wet air oxidation of an aqueous solution of bisphenol A. Oxides were prepared via the sol–gel method and platinum was impregnated onto supports by the wet impregnation technique. Characterizations of the catalysts were performed by using BET, XRD, FESEM, XPS and elemental analysis techniques. Water samples were analysed by HPLC, TOC and UPLC analytical techniques, in order to study the efficiencies of the used catalysts for the removal of BPA from water. Metal contents of the catalysts as well as the possible leaching of the catalysts materials were analysed by using the ICP-OES technique.

2. Materials and methods

This section presents the preparation and testing procedures of the catalysts. Moreover, the analysing techniques of the water samples and characterization methods of catalysts are described in this chapter.

2.1. Catalytic materials

CeO_2, $Ce_{0.8}Ti_{0.2}O_2$ and $Ce_{0.2}Ti_{0.8}O_2$ oxides were prepared by the sol–gel method as described in detail in Ref. [32], using $Ce(NO_3)_3$ $6H_2O$ (Alfa Aesar 99.5%) and $Ti(OC_4H_9)_4$ (Fluka $\geq$ 97%) as precursor salts. After overnight maturing, excess ethanol and water was evaporated first in a sand bath at 100 °C for 5 h and then in a ventilated oven at 120 °C for 20 h. The grinded supports were then calcined under static air at 500 °C for 2 h.

Platinum catalysts (2.5 wt%) were prepared by wet impregnation followed by dry evaporation of the support in a rotating evaporator using an aqueous solution of $Pt(NO_3)_2(NH_3)_4$ (Alfa Aesar 99.99%) (10 g Pt L^{-1}) as a metallic precursor salt and 8 mL of distilled water per gram of support. The catalysts were dried overnight at 120 °C, calcined at 500 °C for 2 h and finally activated by a reduction under H_2 gas (70 mL min^{-1}) for 3 h at 350 °C to obtain Pt in the metallic state. The abbreviations of the supports and catalysts are given in Table 1.

Table 1. Nomenclature of the supports and 2.5 wt% platinum catalysts.

Supports	Abbreviations for supports	Abbreviations for 2.5 wt% Pt catalysts
CeO_2	C(100)	P/C(100)
$Ce_{0.8}Ti_{0.2}O_2$	CT(80)	P/CT(80)
$Ce_{0.2}Ti_{0.8}O_2$	CT(20)	P/CT(20)

2.2. Catalytic oxidation experiments

Catalytic wet air oxidation was carried out in a 0.3 L stainless steel batch reactor equipped with a magnetically driven stirrer for 3 h (Figure 1). In the beginning of the reaction, 160 mL of aqueous solution of bisphenol A (Sigma Aldrich $\leq$ 99%) with a concentration of 60 mg L^{-1}, pH adjusted to 9 and 2 g L^{-1} of catalyst were introduced to the reactor. The reactor was purged with nitrogen, heated to the reaction temperature (160 °C) and then activated with air at a pressure of 2.0 MPa. Oxidation experiments with all prepared catalysts were performed at least three times.

According to the stoichiometry of oxidation reaction (Eq 1) BPA requires 18 mol O_2/mol of BPA to complete oxidation. However, the solubility of oxygen in water at 160 °C is rather low [33] and hence BPA always remains in excess with respect to oxygen during the oxidation reaction.

$$C_{15}H_{16}O_2 + 18O_2 \rightarrow 15CO_2 + 8H_2O \tag{1}$$
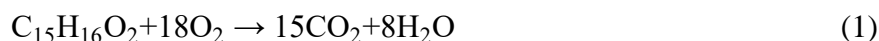
During the reaction, the pressure was kept constant and at regular intervals, water samples were taken from the reactor.
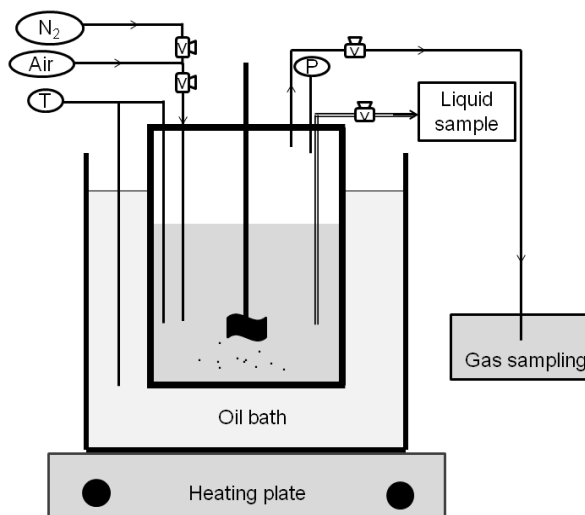
Figure 1. Schematic diagram of the catalytic wet air oxidation reactor system.

2.3. Analytical methods

The concentrations of BPA were analyzed by HPLC using Shimadzu SCL 10A at a wavelength of 226 nm. Waters SunFire C 18, 5 µm particle column (2.1 mm × 100 mm) at 40 ℃ was used for the separation with 45% acetonitrile and 0.1% formic acid solution. The flow rate was set to 0.5 mL min^{-1} after which a 20 µL or 30 µL (BPA concentration < 10 mg L^{-1}) sample was injected. The organic concentration of the water samples was measured by TOC (total organic carbon) according to the procedure described in Ref. [17]. Water samples were filtered by a 0.45 µm cellulose nitrate filter before BPA and TOC measurements in order to remove catalysts particles and suspended solids from the samples. Intermediate products of BPA oxidation were identified using a Waters Synapt G2 High Definition mass spectrometer (MS) with Waters Acquity Ultra Performance Liquid Chromatograph system (UPLC). For pre-treatment, terminal samples (20 mL) were extracted to dichloromethane (8 mL) to concentrate the sample. Acquity UPLCr BEH C18 1.7 µm particle column (2.1 × 100 mm) was used for the separation. Solvent A and B were 0.01% NH_3 and acetonitrile respectively. The initial concentration of solvent B was 5% and was increased linearly during 7 minutes of run to 100%. The flow rate was set at 0.35 mL min^{-1} and 5 µL sample was injected. Possible leaching of the catalyst metals (Pt, Ce, Ti) in water samples and metal content of the fresh and used catalysts were analysed using a Perkin Elmer optical emission spectrometer Optima 5300 DV ICP-OES instrument.

2.4. Characterization of catalysts

The specific surface areas of the fresh and used catalysts were determined by nitrogen adsorption–desorption isotherms at −196 ℃ with a Micromeritics ASAP 2020 analyser. The specific surface area of the samples was calculated by applying the BET theory to nitrogen adsorption data within the 0.03–0.31 p/p$_0$ range. BJH method was used to calculate the pore volumes and pore sizes of the catalysts.

Diffractograms of the catalysts were determined by X-ray powder diffraction (XRD) experiments performed on a PANalytical X'Pert Pro X-ray diffraction system using Cu $K_{\alpha 1}$ radiation (λ = 0.15406 nm). Data was collected in the 2θ range between 20 ° and 90 ° at 0.017 ° intervals with 1.22 s count accumulation per step. Diffractograms were identified by comparison with the PDF database from the International Centre for Diffraction Data (ICDD) [34]. The average crystallite sizes (D) were calculated using the Scherrer equation (Eq 2).

$$D = \frac{K\lambda_{K\alpha}}{\beta_c cos\theta} \qquad (2)$$

In Eq 2, K is the shape factor (0.9), $\lambda_{K\alpha}$ is the wavelength of Cu $K_{\alpha 1}$ radiation (0.15406 nm), β_c is the full width high medium (rad) and θ is the Bragg angle for the considered peak (rad).

The morphology of fresh and used catalysts were investigated by field emission scanning electron microscopy (FESEM) equipped with an energy-dispersive X-ray spectroscopy (EDS) using a Zeiss ULTRA plus microscope. X-ray photoelectron spectroscopy (XPS) analyses were performed on the ESCALAB 250Xi spectrometer (Thermo Fisher Scientific) using monochromatic Al Kα radiation source (1486.7 eV) operated at 20 mA and 15 kV. Due to the charging of the catalysts samples during XPS experiment, Ce 3d u ‴ peak at 916.7 eV was used for the charge correction of the XPS spectra. The Ce 3d u ‴ peak has been generally used to compensate for sample charging in the ceria XPS studies [35,36]. CasaXPS processing software was used for the spectral analysis. The carbon content of the fresh and used catalysts was determined by Thermo Scientific Flash^{TM} 2000 organic elemental analyser (OEA) in order to investigate the amount of possible carbonaceous deposits on the surface of catalysts.

3. Results and discussion

This section summarizes the characterization results (both fresh and used supports and Pt catalysts) and the outcomes from oxidation experiments.

3.1. Specific surface area and X-ray diffraction

Table 2 summarizes the average crystallite size, BET surface area and average pore width of the fresh catalysts. The average crystallite size of C(100) is about 9.2 nm. The adding of smaller amounts of Ti to C(100) decreases the average crystallite size to 8.1 nm (CT(80)) due to the smaller ionic radius of Ti^{4+} (0.68 Å) compared to Ce^{4+} (0.97 Å) [26]. However, there is no change in the specific surface area.

X-ray diffractogram of C(100) sample (Figure 2) calcinated at 500 °C shows the presence of cerium oxide as indicated by the diffraction peaks (marked with #) at about 2θ = 28.5°, 33.1°, 47.5°, 56.3 °, 59.1 °, 69.4 °, 76.7 ° and 79.1 ° corresponding to the planes of the typical face-centered cubic structure of CeO_2 (JCPDS: 01-081-0792) [34].

Table 2. Average crystallite size, BET surface area and average pore width of fresh supports and Pt catalysts.

Sample	Crystallite size [nm]	Surface area [$m^2\ g^{-1}$]	Pore width [nm]
C(100)	9.2	98	12.3
CT(80)	8.1	96	7.5
CT(20)	[a]	194	3.6
P/C(100)	9.1	91	12.6
P/CT(80)	8.2	83	7.8
P/CT(20)	[a]	137	4.4

[a] Determination of the crystallite size is not possible according to the Scherrer equation due to the asymmetric diffraction peaks of the support.
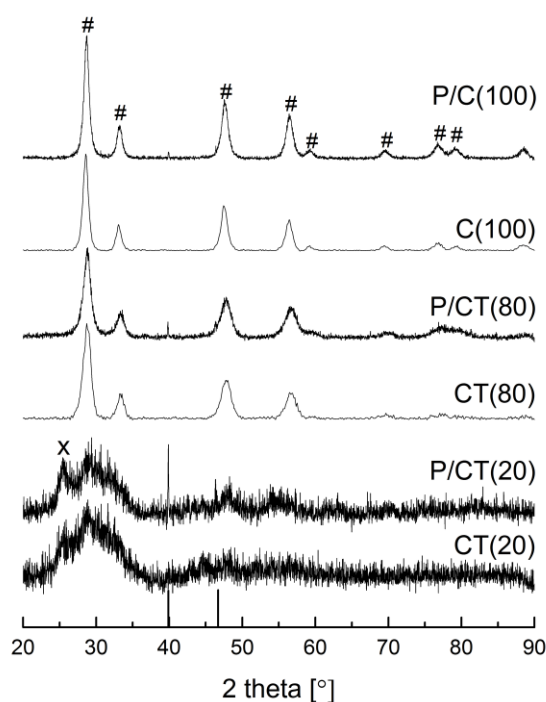

Figure 2. X-ray diffractograms of fresh supports and Pt catalysts. (#) PDF: 01-081-0792 (CeO_2); (x) PDF: 01-089-4921 (TiO_2); (—) PDF: 00-004-0802 (Pt).

When adding small amounts of titanium to CeO_2, the fluorine-type structure is preserved and no relevant Ti peaks is observed by XRD on CT(80) suggesting the incorporation of Ti ions in the cubic lattice to form an homogeneous Ce–Ti–O solid solution. In the X-ray diffractogram of CT(20) (Figure 2) a weak peak at diffraction angle of 25.5 ° could be attributed to anatase titania (JCPDS: 01-089-4921) [34] whilst CeO_2 particles tend not integrate the crystalline phase and CeO_2 appears as an amorphous. This could be due to the insertion of Ti ions into the CeO_2 lattice and replacement of Ce ions. As a coincidence, the long range order structure of the CeO_2 crystal is destroyed which restrains the increasing of the CeO_2 particles [25,26]. Although the crystallite size of CT(20) is not

detected due to the asymmetric diffraction peaks, according to the large surface area of support the crystallite size of CT(20) has decreased (Table 2). In the amorphous structure large lattice distortion is predominated which also explains the large surface area of the CT(20) support [37]. The smaller surface area of CT(80) might be due to a partial destruction of the ordering of TiO_2 or a blockage of the pore entrance [38]. Increasing Ce content may also lead to the segregation of CeO_2 [39]. Moreover, X-ray diffractograms of the platinum catalysts (Figure 2) showed two peaks of platinum at diffraction angles of 39.9 ° and 46.3 ° (marked with —) which are characteristic to metallic platinum (JCPDS: 00-004-0802) [34,40,41]. Both diffraction peaks of platinum are clearly seen in the diffractograms of P/CT(80) and especially in P/CT(20) but in P/C(100) only the highest peak at 2θ 39.9 ° can be observed. This refers to the strong interaction of the active metal and support. Furthermore, no change in the X-ray diffractograms of P/C(100) and P/CT(80) (Figure 2) can be observed due to the introduction of 2.5 wt% platinum whilst in the X-ray diffractogram of P/CT(20) the peak at 2θ 25.5° attributed to anatase titania is stronger than in CT(20). This could be due to the thermal treatments, i.e., calcination and following reduction of Pt catalysts.

3.2. XPS analysis

An example of Ti 2p spectrum can be seen in Figure 3 while Table 3 describes the Ti 2p binding energies of all Ti containing catalysts. The binding energies of Ti $2p_{3/2}$ at about 457 eV and Ti $2p_{1/2}$ at about 463 eV (Table 3) correspond to TiO_2 in Ce–Ti supports and Pt catalysts [26,39].

The Ce 3d XPS spectra of CT(20) and P/CT(20) are seen in Figure 4. The complicated spectra can be resolved into eight components marked with v and u which corresponds to spin-orbit coupling of $3d_{5/2}$ and $3d_{3/2}$ states respectively. The peaks denoted by v and v ″ could be attributed to the mixing of $3d^9 4f^2 (O2p^4)$ and $3d^9 4f^1 (O2p^5)$ Ce^{4+} final states and v ‴ to the $3d^9 4f^0 (O2p^6)$ Ce^{4+} final state. In addition, the peak marked with v ′ is associated to the $3d^9 4f^2 (O2p^6)$ Ce^{3+} final state. The series of $3d_{3/2}$ level peaks denoted by u can be explained in the same way [42,43].
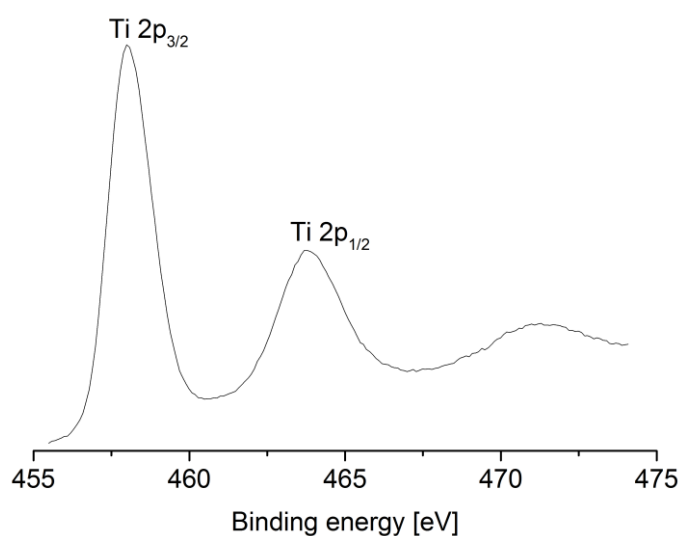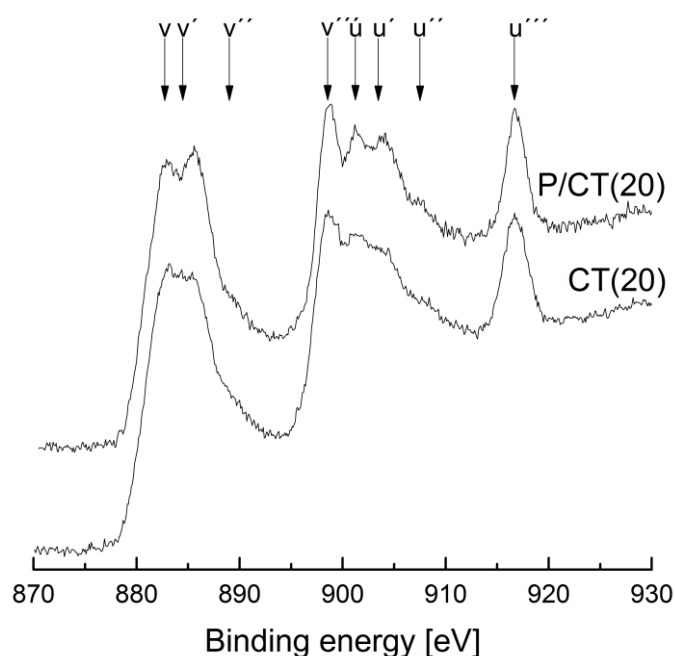

Figure 3. XPS Ti 2p spectrum of P/CT(20).

Table 3. XPS Ti 2p and Ce 3d data for fresh samples.

Sample	Binding energy [eV]			
	Ti		Ce	
	$2p_{3/2}$	$2p_{1/2}$	$3d_{5/2}$ (v)	u ´´´[%]
C(100)	-	-	882.1	13.48
CT(80)	457.4	463.2	882.0	13.69
CT(20)	457.4	463.3	882.1	9.44
P/C(100)	-	-	882.3	14.70
P/CT(80)	457.1	463.0	882.3	14.40
P/CT(20)	457.6	463.3	882.4	8.68

Figure 4. XPS Ce 3d spectra of CT(20) and P/CT(20). Peaks marked by v and u are from the $3d_{5/2}$ and $3d_{3/2}$ states respectively.

Considering Table 3, the binding energies of v peaks for the pure supports and Pt catalysts are in good agreement with existing reported data [44,45]. The ratio of intensity of u ´´´peak to the total Ce 3d intensity depends on the Ce^{4+}/Ce^{3+} ratio, and hence the relative amount of Ce^{4+} present on the surface of the catalyst is the area under u ´´´relative to the total area under the Ce 3d spectrum [42]. As shown in Table 3, for CeO_2 and Ce richer samples the u ´´´is around 13–14% while with Ti richer samples the relative amount of Ce^{4+} has decreased to around 9%. Moreover, u ´and v ´peaks are clearly present in the Ce 3d spectra of CT(20) and P/CT(20) in Figure 4 indicating that the addition of larger amounts of titanium to the CeO_2 lattice increases the amount of Ce^{3+} on the surface of these catalysts [26]. However, a certain amount of Ce^{3+} has probably formed during XPS analysis due to the photoreduction of Ce^{4+} ions which was demonstrated in the study of Larsson and Andersson [46].

For Ce–Ti catalysts increasing the analysis time, the decrease in the area ratio between u ´´´peak to the total Ce 3d region was observed while at the same time, u ´and v ´peaks were increased. This phenomenon shows the reduction of Ce^{4+} to Ce^{3+} during XPS analysis. Furthermore, amorphous Ce–Ti mixed oxides prepared by the sol–gel method have been found to be more easily reduced due to photoreduction than the crystalline form and physical mixture of these oxides [36,39,45].

An example of the O 1s spectrum (C(100)) can be seen in Figure 5. The spectrum is composed of three peaks referred as lattice oxygen (O I), chemisorbed oxygen (O II) and oxygen of CO_3^{2-} groups (O III) [26,47,48]. The O 1s peaks at about 527.6–529.4 eV (Table 4) could be attributed to the lattice oxygen while the smaller O 1s peaks around 528.7–530.2 eV belong to the chemisorbed oxygen for C(100), CT(80), CT(20), P/C(100), P/CT(80) and P/CT(20) catalysts [26,45]. O III is present only in the C(100), P/CT(80) and P/CT(20) samples.
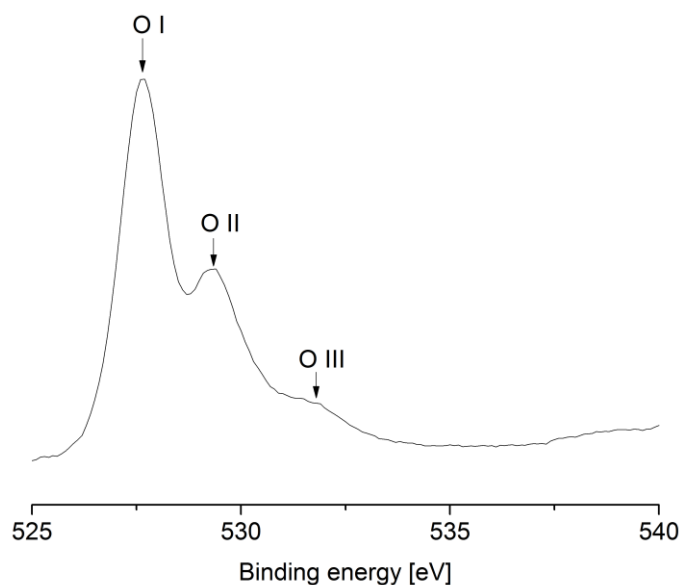

Figure 5. XPS O 1s spectrum of C(100) support.

Table 4. XPS O 1s data for fresh supports and Pt catalysts.

Sample	Binding energy [eV]			O/O T [%]		
	O I	O II	O III	O I/O T	O II/O T	O III/O T
C(100)	527.6	529.3	531.1	53.63	26.40	14.97
CT(80)	528.5	529.6	-	67.47	32.53	-
CT(20)	529.0	530.1	-	77.92	22.08	-
P/C(100)	527.5	528.7	-	53.02	46.98	-
P/CT(80)	528.1	529.2	531.6	46.68	38.91	14.41
P/CT(20)	529.4	530.2	532.5	61.82	30.63	7.55

As shown in Table 4, the amount of lattice oxygen is larger than the amount of chemisorbed oxygen in all samples. In CT(80) and P/CT(80) containing smaller amounts of titanium the chemisorbed oxygen content is bigger than in CT(20) and P/CT(20) with higher amounts of titanium.

This is not in agreement with the Ce^{3+} content of catalysts (Table 3). Typically, reduced Ce can form vacancies and unsaturated chemical bonds that create a charge imbalance on the surface of these catalysts, which make the existence of the chemisorbed oxygen possible on the catalyst surface. However, Ti^{4+} with a smaller ionic radius than Ce can enter the CeO_2 lattice and substitute for Ce^{3+}. This might affect the charge balance of the surface and lead to the decrease in the amount of chemisorbed oxygen on the catalyst surface which probably explains the smaller amounts of O II specie in the Ti rich catalysts. However, the addition of platinum increased the amount of chemisorbed oxygen in all catalysts. Therefore, platinum can activate the oxygen species' migration on the support and further improve the activity of these catalysts [22,49]. Chemisorbed oxygen has a very important role in the oxidation reaction and so different amounts can affect the activity of Ce and Ce–Ti catalysts [26].

The XPS binding energy values of Pt 4f spectra (not shown) of reduced platinum catalysts are given in Table 5. All platinum catalysts show several peaks in the Pt 4f region due to the multiple oxidation state of the samples. The Pt $4f_{7/2, \ 5/2}$ peaks at 70.8–71.1 eV and 73.4–76.6 eV could be attributed to metallic Pt as well as Pt $4f_{7/2, \ 5/2}$ peaks at 71.4–72.4 eV, 75.3–76.2 eV and 74.1–74.6 eV, 76.3–77.2 eV could be assigned to Pt^{2+} and Pt^{4+} respectively [50]. Considering the binding energy values of Pt catalysts in Pt 4f spectra, the samples containing more ceria has slightly higher binding energy than the P/CT(20) catalyst (Table 5). This shifting of the binding energy values could be due to the interaction of the platinum with ceria and further electronic polarization of the platinum precursor clusters [50]. Moreover, the shifting of the binding energies has been found to be strongly dependent on the cerium content of the Pt catalysts [51]. Therefore, P/C(100) and P/CT(80) catalysts with high Ce content show higher Pt $4f_{7/2}$ binding energy than P/CT(20). Despite the reduction of the Pt catalysts, platinum is found to be dispersed mostly in 2+ and 4+ (>80%) oxidation states in all samples. Therefore, the strong interaction between active metal and support prevented platinum to reduce in the metallic state [50] in the used reaction conditions.

Table 5. Binding energies of different platinum species observed from Pt 4f spectra of fresh catalysts.

Sample	Binding energy of $4f_{7/2}$ [eV]		
	Pt^0	Pt^{2+}	Pt^{4+}
P/C(100)	70.2	72.8	74.9
P/CT(80)	71.0	72.6	74.4
P/CT(20)	70.9	72.1	74.3

3.3. ICP-OES and FESEM-EDS analysis

FESEM-EDS was used for the analysing the morphology and composition of catalysts' surface. In the FESEM image of P/C(100) (Figure 6a) typical porous structure of ceria [52] with a wide particle size can be observed whilst in P/CT(20) catalyst particles were characterized by an angular shape (Figure 6b).
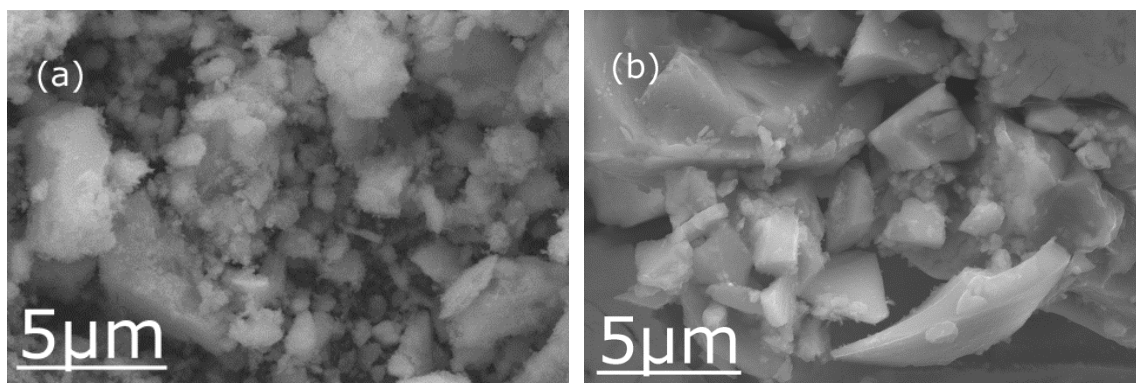
Figure 6. FESEM images of fresh P/C(100) (a) and P/CT(20) (b) catalysts.

Table 6 summarizes the wt% of the catalyst metals determined by ICP-OES and FESEM-EDS. Ce and Ti content of the supports are in good agreement in the target values of these metals in the catalysts. After impregnation of the active metal to the supports, no effect to the wt% of Ce and Ti can be noticed. Moreover, Ce and Ti seem to be well dispersed on the surface as well as in the bulk of the catalysts since both analysing techniques give quite similar results. Analysing the platinum content of the catalysts by ICP-OES, the wt% of the active metal is quite near the target value (2.5 wt%). However, according to FESEM-EDS analysis, the dispersion of Pt is not homogeneous, except in P/CT(20). This might be due to a larger particle size of the Ti richer Pt catalyst (Figure 6b) compared to the smaller particle size of P/C(100) (Figure 6a).

Table 6. Wt% of catalyst metals of fresh samples analysed by ICP-OES and FESEM-EDS.

Sample	Ce [wt%]			Ti [wt%]			Pt [wt%]	
	Target	ICP	EDS	Target	ICP	EDS	ICP	EDS
C(100)	81	84	86	-	-	-	-	-
CT(80)	73	76	70	6.2	8.5	8.6	-	-
CT(20)	29	31	22	39	46	41	-	-
P/C(100)	81	77	81	-	-	-	2.2	0.7
P/CT(80)	73	71	70	6.2	7.6	7.3	2.2	4.2
P/CT(20)	29	29	28	39	42	37	2.4	2.2

3.4. Catalytic wet air oxidation of bisphenol A

The thermal stability of the bisphenol A aqueous solution (60 mg L^{-1}) at operating conditions (160 °C, 2.0 MPa of air) was first evaluated. No removal of BPA and TOC was observed (not shown) after 3 h of experiment. Catalytic wet air oxidation experiments were carried out with both pure supports and with active metal. All catalysts were active in the abatement of BPA (Table 7). The oxidation reaction was very fast: After 30 minutes reaction the lowest abatement of BPA was already 50% (C(100)) and the highest almost 90% (P/C(100)) (Figures 7 and 8). No significant differences between used supports in the BPA removal were observed and after 3 h experiment, the BPA

abatement was around 75%. By adding active metal to the supports, the highest BPA removal (97%) was achieved with the P/C(100) catalyst. The activity order of the catalysts was P/C(100) > P/CT(80) > P/CT(20) > C(100) > CT(20) > CT(80). Surprisingly, the activity order of the catalysts was not in agreement to the BET surface areas of the samples (Table 2). The lower activity of the Ti richer catalysts with higher BET surface area could be due to the lower amount of chemisorbed oxygen of these catalysts (Table 4). In fact, the order of the activity was almost the same as that of the surface concentration of chemisorbed oxygen for Pt catalysts.
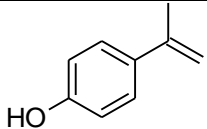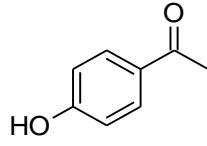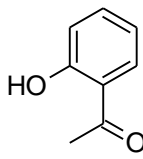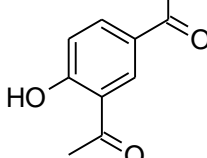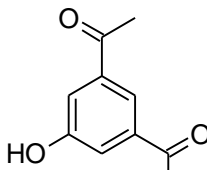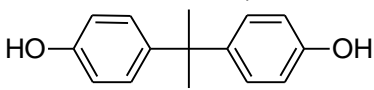
In the TOC conversions of the oxidation reactions (Table 7), no significant differences between the used catalysts in the organic concentration removal were observed. The TOC abatement was slightly higher with Pt catalysts than with pure supports.

The lower removal of TOC than BPA was assumed to be due to the forming of by-products in the BPA oxidation reaction. Therefore, a qualitative analysis was performed by UPLC-MS to the oxidized water samples. According to the obtained mass spectra (not shown), five different by-products in addition of BPA were identified from the terminal water samples from which compounds B and C existed in two isomers (Table 8). The products A, i.e., 4-(prop-1-en-2-yl)phenol and B1 (1-(4-hydroxyphenyl)ethan-1-one, i.e., p-hydroxyacetophenone) were detected also as degradation products in the photocatalytic treatment of BPA [53]. Moreover, p-hydroxyacetophenone was identified as a main by-product in the CWAO of BPA by titanate nanotube-based catalysts in addition of acetic and formic acids [54] which were not detected in the UPLC-MS analysis. However, with the low BPA concentration and therefore, the low concentration of intermediates, major amount of intermediates could be absorbed on the catalyst's surface and not observed in the liquid phase. Although carboxylic acids were not detected in the UPLC analysis, the pH values of pure supports catalysed oxidized water samples were near five which refers the forming of formic and acetic acids. Typically, these short chain carboxylic acids are refractory for total oxidation to CO_2 and water with metal oxide catalysts [26]. Further, compound C with the molecular weight of 178 g mol^{-1} existed in two isomers 1,1'-(4-hydroxy-1,3-phenylene)di(ethan-1-one) (product C1) and 1,1'-(5-hydroxy-1,3-phenylene)di(ethan-1-one) (product C2) was not detected in the earlier studies related to the oxidation of BPA.

Table 7. BPA and TOC removal ($\pm 2.0\%$) after 3 h CWAO for C(100), CT(80) and CT(20) catalysts with and without Pt. Temperature 160 °C, air pressure 2.0 MPa, concentration of the catalyst 2 g L^{-1}.

Sample	BPA removal [%]	TOC removal [%]
C(100)	77	52
CT(80)	71	47
CT(20)	76	49
P/C(100)	97	59
P/CT(80)	95	60
P/CT(20)	90	58

Table 8. UPLC-MS data of the by-products detected in BPA solution treated by CWAO.

Compound	Molecular weight [g·mol⁻¹]	Formula	Tentative structure
A	134	$C_9H_{10}O$	
B1	136	$C_8H_8O_2$	
B2	136	$C_8H_8O_2$	
C1	178	$C_{10}H_{10}O_3$	
C2	178	$C_{10}H_{10}O_3$	
BPA	227	$C_{15}H_{16}O_2$	

3.5. Kinetic modelling of oxidation reaction

The kinetics of BPA removal was modelled according to the pseudo-first order rate-law. The measured data was fitted by using a standard non-linear least squares algorithm, Eq 3,

$$R(t) = R_{\text{Tot}}(1 - e^{-kt}) \tag{3}$$

in which total removal (R_{Tot}) and rate constant (k) were used as fitting parameters. The term "t" was the oxidation time. The calculated R^2 values and residual analysis were used as evaluating parameters for the goodness of the fit. Figure 7 shows both the experimental (symbols) and fitted (lines) BPA removals as a function of reaction time for pure supports. The possible rate constants for C(100), CT(80) and CT(20) catalysts were 0.0387, 0.0541 and 0.0740 min⁻¹, respectively. Therefore, the addition of more titania to the support increased the reaction rate in the CWAO of BPA and the kinetic constant of CT(20) was almost 2 times higher as that of C(100). The fitted and observed abatements of BPA for Pt catalysts are presented in Figure 8 and the calculated rate constants were 0.0810 (P/C(100)), 0.0322 (P/CT(80)) and 0.0324 min⁻¹ (P/CT(20)). On the contrary to the supports, the addition of active metal improved the reaction rate of the CWAO of BPA only with P/C(100) and the kinetic constant of P/C(100) was 2.5 times higher than that with P/CT(80) and P/CT(20).
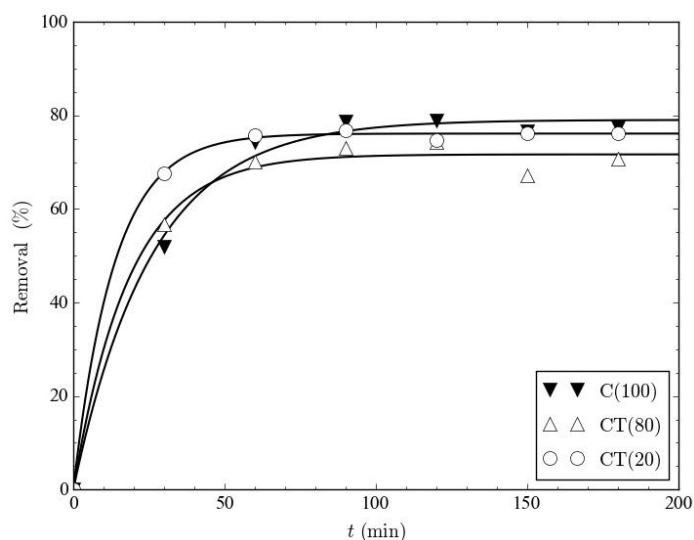
Figure 7. Bisphenol A removal as a function of oxidation time for C(100), CT(80) and CT(20) catalysts. Temperature 160 °C, air pressure 2.0 MPa, concentration of the catalyst 2 g L^{-1}. Solid lines present the fitted and symbols the experimental results.
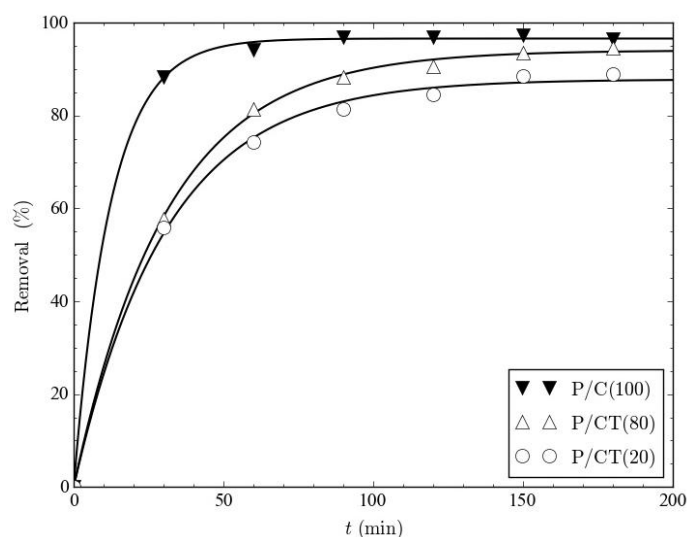

Figure 8. Bisphenol A removal as a function of oxidation time for P/C(100), P/CT(80) and P/CT(20) catalysts. Temperature 160 °C, air pressure 2.0 MPa, concentration of the catalyst 2 g L^{-1}. Solid lines present the fitted and symbols the experimental results.

3.6. Characterization of used catalysts

After oxidation reaction of BPA, the diffraction peaks characteristics to cerium oxide have shown no changes in both used supports and Pt catalysts (Figure 9). Furthermore, the platinum peak at 2θ 39.9 ° is obvious in all used Pt catalysts. However, in the diffractograms of used CT(20) and P/CT(20) four clear peaks at a 2θ values at approx. 25 °, 38 °, 48 ° and 54 ° can be seen while only weak peak at diffraction angle 25 ° is obvious in fresh samples (Figure 2). The diffraction peaks (marked with x) at 25.5 °, 38.1 °, 48.0 ° and 54.4 ° for CT(20) and P/CT(20) respectively, can be

attributed to anatase titania (JCPDS: 01-089-4921) [34]. No rutile titania peaks are detected and so the TiO_2 phase exists as an anatase structure in the used samples.

The crystallite sizes of used C(100), CT(80), P/C(100) and P/CT(80) catalysts are in the same range (8.2–9.2 nm) to the fresh samples (Table 2). The structure of the used CT(20) and P/CT(20) is still amorphous and the faint scattering of the diffractograms (Figure 9) prevents the exact determination of the crystallite size of these catalysts. Moreover, the surface area of the used Ce and low amount of Ti containing samples stayed quite steady and the lowest decrease occurred in C(100) (6.1%) and P/CT(80) (7.2%) samples. However, after oxidation reaction the surface area of CT(20) and P/CT(20) decreased 55 and 36%, respectively. Therefore, the amount of accumulated carbon on the surface of the catalysts was examined by elemental analysis for both fresh and used catalysts (Table 9).

According to the results, low amount of carbon had accumulated on the surface of fresh catalysts even before the oxidation reaction of BPA. However, this was probably due to the absorbed CO_2 on these samples. Moreover, the addition of Ti to the supports slightly prevented the adsorption of carbonaceous molecules on the fresh catalysts. After oxidation reaction, rather low carbon contents were observed on the surface of the used catalysts. In fact, in part of the catalysts the initial carbonaceous deposits had actually removed during CWAO of BPA. Additionally, the accumulation of carbon during CWAO of BPA was more intensive in pure supports than samples with active metal. However, it is obvious according to elemental analysis that carbonaceous deposits were not responsible for the loss of specific surface area of CT(20) and P/CT(20). Therefore, the phase changes observed in X-ray diffractograms after oxidation reaction caused the decrease in the surface area of these samples. Further, P/C(100) and P/CT(80) which were the most active catalysts in the CWAO of BPA, in addition of oxidising the organic compounds from treated effluent, removed also the initial carbonaceous deposits from catalysts surface.
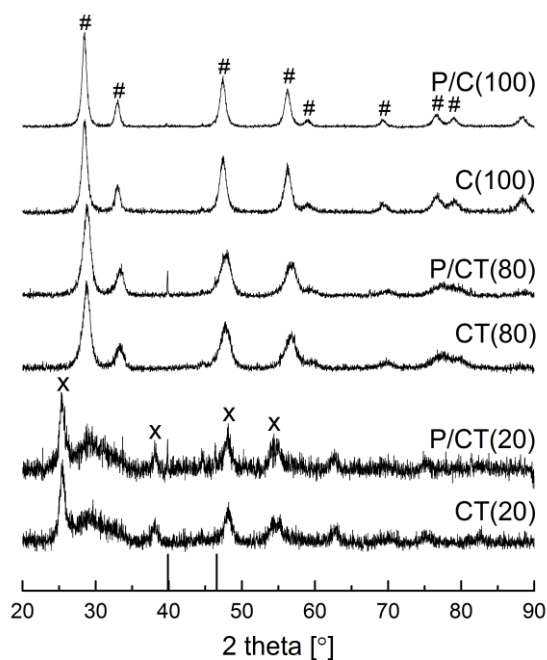

Figure 9. X-ray diffractograms of used supports and Pt catalysts. (#) PDF: 01-081-0792 (CeO$_2$); (—) PDF: 00-004-0802 (Pt); (x) PDF: 01-089-4921 (TiO$_2$).

Table 9. Carbon content on the surface of the fresh and used catalysts studied in the CWAO of BPA.

Sample	fresh [mg C g^{-1}]	used [mg C g^{-1}]
C(100)	6.9	13.2
CT(80)	4.6	9.5
CT(20)	6.0	5.5
P/C(100)	8.8	5.5
P/CT(80)	5.2	4.3
P/CT(20)	2.1	10.4

Additionally, according to the metal content analysis of used catalysts by ICP-OES the amount of Ce, Ti and Pt stayed quite steady and no leaching of these metals occurred in terminal water samples after oxidation reaction.

Consequently, according to the post characterization of the catalysts, phase composition of Ce and small amount of Ti containing samples stayed steady and no large changes in the surface area of these samples occurred after CWAO of BPA. However, in spent CT(20) and P/CT(20) anatase titania peaks appeared in XRD analysis and 55 and 36% decrease in the surface areas was observed. Therefore, P/CT(80) was the most stable catalysts in the CWAO of BPA due to the negligible loss of surface area and unchangeable phase structure. Moreover, no accumulation of carbonaceous deposits on the surface of the P/CT(80) were observed after oxidation reaction.

4. Conclusions

Platinum supported on sol–gel prepared CeO_2, $Ce_{0.8}Ti_{0.2}O_2$ and $Ce_{0.2}Ti_{0.8}O_2$ were used as catalysts in the catalytic wet air oxidation of an aqueous solution of bisphenol A. The addition of Ti to CeO_2 affects the surface properties of the mixed oxides. In CT(20) the higher Ti content turns CeO_2 into an amorphous and increases the specific surface area of the sample. However, CWAO of BPA is not a surface area specific reaction. The oxidation reaction was followed the pseudo-first order rate law and the highest abatement of BPA was achieved with P/C(100) and P/CT(80) catalysts, 97 and 95% respectively. The excellent activity of these catalysts is to do with the high concentration of chemisorbed oxygen and Ce^{4+} on the surface of the catalysts. Moreover, no phase changes and carbonaceous deposits existed in P/CT(80) and P/C(100) samples after oxidation reaction. Consequently, these catalysts show high potential in the removal of endocrine disrupting chemicals from wastewaters by catalytic wet air oxidation.

Conflict of interest

The authors declare that they have no conflicts of interest.

References

1. Corrales J, Kristofco LA, Steele WB, et al. (2015) Global assessment of bisphenol A in the environment: Review and analysis of its occurrence and bioaccumulation. *Dose-Response* 13: 1559325815598308.
2. Meeker JD, Calafat AM, Hauser R (2010) Urinary bisphenol A concentrations in relation to serum thyroid and reproductive hormone levels in men from an infertility clinic. *Environ Sci Technol* 44: 1458–1463.
3. Hassan ZK, Elobeid MA, Virk P, et al. (2012) Bisphenol A induces hepatotoxicity through oxidative stress in rat model. *Oxid Med Cell Longev* 2012: 194829.
4. Helmestam M, Davey E, Stavreus-Evers A, et al. (2014) Bisphenol A affects human endometrial endothelial cell angiogenic activity *in vitro*. *Reprod Toxicol* 46: 69–76.
5. Li Y, Jin F, Wang C, et al. (2015) Modification of bentonite with cationic surfactant for the enhanced retention of bisphenol A from landfill leachate. *Environ Sci Pollut R* 22: 8618–8628.
6. Rocha S, Domingues V, Pinho C, et al. (2013) Occurrence of bisphenol A, estrone, 17β-estradiol and 17α-ethinylestradiol in Portuguese Rivers. *B Environ Contam Tox* 90: 73–78.
7. Lee CC, Jiang LY, Kuo YL, et al. (2013) The potential role of water quality parameters on occurrence of nonylphenol and bisphenol A and identification of their discharge sources in the river ecosystems. *Chemosphere* 91: 904–911.
8. Kawagoshi Y, Fujita Y, Kishi I, et al. (2003) Estrogenic chemicals and estrogenic activity in leachate from municipal waste landfill determined by yeast two-hybrid assay. *J Environ Monitor* 5: 269–274.
9. Coors A, Jones P, Giesy J, et al. (2003) Removal of estrogenic activity from municipal waste landfill leachate assessed with a bioassay based on reporter gene expression. *Environ Sci Technol* 37: 3430–3434.
10. Lee H, Peart TE, Chan J, et al. (2004) Occurrence of endocrine-disrupting chemicals in sewage and sludge samples in Toronto, Canada. *Water Qual Res J Can* 39: 57–63.
11. Hoigné J, Bader H, Haag WR, et al. (1985) Rate constants of reactions of ozone with organic and inorganic compounds in water—III. Inorganic compounds and radicals. *Water Res* 19: 993–1004.
12. Spivack J, Leib TK, Lobos JH (1994) Novel pathway for bacterial metabolism of bisphenol A. Rearrangements and stilbene cleavage in bisphenol A metabolism. *J Biol Chem* 269: 7323–7329.
13. Marttinen SK, Kettunen RH, Rintala JA (2003) Occurrence and removal of organic pollutants in sewages and landfill leachates. *Sci Total Environ* 301: 1–12.
14. Clara M, Strenn B, Saracevic E, et al. (2004) Adsorption of bisphenol-A, 17β-estradiole and 17α-ethinylestradiole to sewage sludge. *Chemosphere* 56: 843–851.
15. Kondrakov AO, Ignatev AN, Frimmel FH, et al. (2014) Formation of genotoxic quinones during bisphenol A degradation by TiO_2 photocatalysis and UV photolysis: A comparative study. *Appl Catal B-Environ* 160: 106–114.

16. Richard J, Boergers A, vom Eyser C, et al. (2014) Toxicity of the micropollutants bisphenol A, ciprofloxacin, metoprolol and sulfamethoxazole in water samples before and after the oxidative treatment. *Int J Hyg Envir Heal* 217: 506–514.

17. Juhola R, Heponiemi A, Tuomikoski S, et al. (2017) Preparation of novel Fe catalysts from industrial by-products: Catalytic wet peroxide oxidation of bisphenol A. *Top Catal* 60: 1387–1400.

18. Erjavec B, Kaplan R, Djinovic P, et al. (2013) Catalytic wet air oxidation of bisphenol A model solution in a trickle-bed reactor over titanate nanotube-based catalysts. *Appl Catal B-Environ* 132–133: 342–352.

19. Levec J, Pintar A (2007) Catalytic wet-air oxidation processes: A review. *Catal Today* 124: 172–184.

20. Luck F (1999) Wet air oxidation: Past, present and future. *Catal Today* 53: 81–91.

21. Sassi H, Lafaye G, Amor HB, et al. (2017) Wastewater treatment by catalytic wet air oxidation process over Al–Fe pillared clays synthesized using microwave irradiation. *Front Env Sci Eng* 12: 2–7.

22. De Los Monteros AE, Lafaye G, Cervantes A, et al. (2015) Catalytic wet air oxidation of phenol over metal catalyst (Ru, Pt) supported on TiO_2–CeO_2 oxides. *Catal Today* 258: 564–569.

23. Zhang Y, Zhou Y, Peng C, et al. (2018) Enhanced activity and stability of copper oxide/γ-alumina catalyst in catalytic wet-air oxidation: Critical roles of cerium incorporation. *Appl Surf Sci* 436: 981–988.

24. Schmit F, Bois L, Chassagneux F, et al. (2015) Catalytic wet air oxidation of methylamine over supported manganese dioxide catalysts. *Catal Today* 258: 570–575.

25. Yang S, Zhu W, Wang J, et al. (2008) Catalytic wet air oxidation of phenol over CeO_2–TiO_2 catalyst in the batch reactor and the packed-bed reactor. *J Hazard Mater* 153: 1248–1253.

26. Yang S, Zhu W, Jiang Z, et al. (2006) The surface properties and the activities in catalytic wet air oxidation over CeO_2–TiO_2 catalysts. *Appl Surf Sci* 252: 8499–8505.

27. Saroha AK (2017) Treatment of industrial organic raffinate containing pyridine and its derivatives by coupling of catalytic wet air oxidation and biological processes. *J Clean Prod* 162: 973–981.

28. Yadav A, Verma N (2018) Carbon bead-supported copper-dispersed carbon nanofibers: An efficient catalyst for wet air oxidation of industrial wastewater in a recycle flow reactor. *J Ind Eng Chem* 67: 448–460.

29. Kim K, Ihm S (2011) Heterogeneous catalytic wet air oxidation of refractory organic pollutants in industrial wastewaters: A review. *J Hazard Mater* 186: 16–34.

30. Gaálová J, Barbier J, Rossignol S (2010) Ruthenium versus platinum on cerium materials in wet air oxidation of acetic acid. *J Hazard Mater* 181: 633–639.

31. Wang J, Zhu W, He X, et al. (2008) Catalytic wet air oxidation of acetic acid over different ruthenium catalysts. *Catal Commun* 9: 2163–2167.

32. Azalim S, Franco M, Brahmi R, et al. (2011) Removal of oxygenated volatile organic compounds by catalytic oxidation over Zr–Ce–Mn catalysts. *J Hazard Mater* 188: 422–427.

33. Kolaczkowski ST, Plucinski P, Beltran FJ, et al. (1999) Wet air oxidation: A review of process technologies and aspects in reactor design. *Chem Eng J* 73: 143–160.

34. International Centre for Diffraction Data (ICDD) (2013) PDF-4+ powder diffraction database. 12 Campus Boulevard Newton Square, PA 19073-3273, USA.

35. El Fallah J, Hilaire L, Roméo M, et al. (1995) Effect of surface treatments, photon and electron impacts on the ceria 3d core level. *J Electron Spectrosc* 73: 89–103.

36. Park PW, Ledford JS (1996) Effect of crystallinity on the photoreduction of cerium oxide: A study of CeO_2 and Ce/Al_2O_3 catalysts. *Langmuir* 12: 1794–1799.

37. Zhao B, Shi B, Zhang X, et al. (2011) Catalytic wet hydrogen peroxide oxidation of H-acid in aqueous solution with TiO_2–CeO_2 and Fe/TiO_2–CeO_2 catalysts. *Desalination* 268: 55–59.

38. Zhang XH, Luo LT, Duan ZH (2005) Preparation and application of Ce-doped mesoporous TiO_2 oxide. *React Kinet Catal Lett* 87: 43–50.

39. Francisco MSP, Mastelaro VR, Nascente PAP, et al. (2001) Activity and characterization by XPS, HR-TEM, raman spectroscopy, and BET surface area of CuO/CeO_2–TiO_2 catalysts. *J Phys Chem B* 105: 10515–10522.

40. Dipti SS, Chung UC, Chung WS (2007) Characteristics of the carbon nanotubes supported Pt–Ni and Ni electrocatalysts for DMFC. *Met Mater Int* 13: 257–260.

41. Luo N, Fu X, Cao F, et al. (2008) Glycerol aqueous phase reforming for hydrogen generation over Pt catalyst—Effect of catalyst composition and reaction conditions. *Fuel* 87: 3483–3489.

42. Shyu JZ, Weber WH, Gandhi HS (1988) Surface characterization of alumina-supported ceria. *J Phys Chem* 92: 4964–4970.

43. Laachir A, Perrichon V, Badri A, et al. (1991) Reduction of CeO_2 by hydrogen. Magnetic susceptibility and Fourier-transform infrared, ultraviolet and X-ray photoelectron spectroscopy measurements. *J Chem Soc Faraday Trans* 87: 1601–1609.

44. Galtayries A, Sporken R, Riga J, et al. (1998) XPS comparative study of ceria/zirconia mixed oxides: Powders and thin film characterisation. *J Electron Spectrosc* 88–91: 951–956.

45. Dauscher A, Hilaire L, Le Normand F, et al. (1990) Characterization by XPS and XAS of supported Pt/TiO_2–CeO_2 catalysts. *Surf Interface Anal* 16: 341–346.

46. Larsson PO, Andersson A (1998) Complete oxidation of CO, ethanol, and ethyl acetate over copper oxide supported on titania and ceria modified titania. *J Catal* 179: 72–89.

47. Larachi F, Pierre J, Adnot A, et al. (2002) Ce 3d XPS study of composite $Ce_xMn_{1-x}O_{2-y}$ wet oxidation catalysts. *Appl Surf Sci* 195: 236–250.

48. Alifanti M, Baps B, Blangenois N, et al. (2003) Characterization of CeO_2–ZrO_2 mixed oxides. comparison of the citrate and sol–gel preparation methods. *Chem Mater* 15: 395–403.

49. Bedrane S, Descorme C, Duprez D (2002) Investigation of the oxygen storage process on ceria- and ceria–zirconia-supported catalysts. *Catal Today* 75: 401–405.

50. Bera P, Priolkar KR, Gayen A, et al. (2003) Ionic dispersion of Pt over CeO_2 by the combustion method: Structural investigation by XRD, TEM, XPS, and EXAFS. *Chem Mater* 15: 2049–2060.

51. Tiernan MJ, Finlayson OE (1998) Effects of ceria on the combustion activity and surface properties of Pt/Al_2O_3 catalysts. *Appl Catal B-Environ* 19: 23–35.

52. Hori CE, Permana H, Ng KYS, et al. (1998) Thermal stability of oxygen storage properties in a mixed CeO_2–ZrO_2 system. *Appl Catal B-Environ* 16: 105–117.

53. Ohko Y, Ando I, Niwa C, et al. (2001) Degradation of bisphenol A in water by TiO_2 photocatalyst. *Environ Sci Technol* 35: 2365–2368.

54. Mezohegyi G, Erjavec B, Kaplan R, et al. (2013) Removal of bisphenol A and its oxidation products from aqueous solutions by sequential catalytic wet air oxidation and biodegradation. *Ind Eng Chem Res* 52: 9301–9307.